

# Physics-Conditioned Diffusion Models for Lattice Gauge Theory

---

Qianteng Zhu<sup>a,b</sup>, Gert Aarts<sup>c</sup>, Wei Wang<sup>a,d</sup>, Kai Zhou<sup>e,f</sup> and Lingxiao Wang<sup>b</sup>

<sup>a</sup>State Key Laboratory of Dark Matter Physics, Shanghai Key Laboratory for Particle Physics and Cosmology, Tsung-Dao Lee Institute and School of Physics and Astronomy, Shanghai Jiao Tong University, Shanghai 200240, China

<sup>b</sup>Interdisciplinary Theoretical and Mathematical Sciences Program (*iTHEMS*), RIKEN, Wako, Saitama 351-0198, Japan

<sup>c</sup>Department of Physics, Swansea University, SA2 8PP, Swansea, United Kingdom

<sup>d</sup>Southern Center for Nuclear-Science Theory (SCNT), Institute of Modern Physics, Chinese Academy of Sciences, 96 South Sihuan Rd. Huicheng District, Huizhou 516000, Guangdong, China

<sup>e</sup>School of Science and Engineering, The Chinese University of Hong Kong, Shenzhen (CUHK-Shenzhen), Guangdong, 518172, China

<sup>f</sup>Frankfurt Institute for Advanced Studies, Ruth Moufang Strasse 1, D-60438, Frankfurt am Main, Germany

E-mail: [zhuqianteng@sjtu.edu.cn](mailto:zhuqianteng@sjtu.edu.cn), [g.aarts@swansea.ac.uk](mailto:g.aarts@swansea.ac.uk),  
[wei.wang@sjtu.edu.cn](mailto:wei.wang@sjtu.edu.cn), [zhoukai@cuhk.edu.cn](mailto:zhoukai@cuhk.edu.cn), [lingxiao.wang@riken.jp](mailto:lingxiao.wang@riken.jp)

**ABSTRACT:** We develop diffusion models for simulating lattice gauge theories, where stochastic quantization is explicitly incorporated as a physical condition for sampling. We demonstrate the applicability of this novel sampler to U(1) gauge theory in two spacetime dimensions and find that a model trained at a small inverse coupling constant can be extrapolated to larger inverse coupling regions without encountering the topological freezing problem. Additionally, the trained model can be employed to sample configurations on different lattice sizes without requiring further training. The exactness of the generated samples is ensured by incorporating Metropolis-adjusted Langevin dynamics into the generation process. Furthermore, we demonstrate that this approach enables more efficient sampling of topological quantities compared to traditional algorithms such as Hybrid Monte Carlo and Langevin simulations.

---

## Contents

<b>1</b>	<b>Introduction</b>	<b>1</b>
<b>2</b>	<b>Simulation of Lattice Gauge Fields</b>	<b>3</b>
2.1	Hybrid Monte Carlo	3
2.2	Topological Charge Freezing	4
<b>3</b>	<b>Diffusion Model and Score Matching</b>	<b>5</b>
3.1	Diffusion Models	5
3.2	Noise Conditional Score Networks	6
<b>4</b>	<b>Physics-Conditioned Sampler</b>	<b>8</b>
4.1	Physics-Conditioned Score Function	8
4.2	Metropolis-Adjusted Annealed Langevin Algorithm	9
<b>5</b>	<b>Numerical Experiments</b>	<b>11</b>
5.1	Performance in the Unfrozen Region	11
5.1.1	Training and validation	11
5.1.2	Generation at different lattice sizes	11
5.2	Generation in the Frozen Region	12
5.2.1	Mitigate freezing	12
5.2.2	Generation at different lattice sizes and couplings	13
<b>6</b>	<b>Summary and Outlook</b>	<b>14</b>
<b>A</b>	<b>Langevin Sampler</b>	<b>16</b>
<b>B</b>	<b>Autocorrelation Time</b>	<b>17</b>
<b>C</b>	<b>Analytical Results</b>	<b>18</b>
<b>D</b>	<b>Likelihood Estimation</b>	<b>19</b>

---

## 1 Introduction

Lattice field theory is a discretization method for quantum field theory in which fields are defined on a spacetime lattice. The fundamental idea is to employ the Euclidean path integral formulation, representing the behaviour of quantum fields as a weighted sum over all possible field configurations. Observables are then defined as

$$\langle O \rangle = \frac{1}{Z} \int \mathcal{D}\phi O[\phi] e^{-S_E[\phi]}, \quad Z = \int \mathcal{D}\phi e^{-S_E[\phi]}, \quad (1.1)$$

where  $Z$  is the partition function,  $S_E[\phi]$  is the discretized Euclidean action of the field, and  $\phi$  represents a field variable  $\phi(x)$  defined at spacetime position  $x$ .

Direct computation of path integrals is often challenging, particularly in higher dimensional systems or strongly-coupled regimes. To achieve an unbiased estimation of  $\langle O \rangle$ , traditional numerical simulation methods, such as the Markov Chain Monte Carlo (MCMC) algorithm, sample field configurations according to the probability distribution,

$$p[\phi] = \frac{1}{Z} e^{-S_E[\phi]}. \quad (1.2)$$

Despite the success of MCMC in simulating lattice field theories, one often encounters the issue of critical slowing down [1]. This phenomenon occurs when the correlation time of a system increases significantly as it approaches a critical point in parameter space, leading to escalating computational costs and insufficient diversity in the sampled configurations. Although alternative methods [2–9] have been proposed to mitigate critical slowing down in specific models, it remains a longstanding challenge in lattice simulations of Quantum Chromodynamics.

Generative models in machine learning (ML), which aim to map samples from a simple prior distribution to a complex physical distribution, have shown great promise in addressing challenges such as critical slowing down in lattice field theory. Recent advancements in generative models have introduced novel approaches for lattice field theory simulations [10–12]. Among these, flow-based models have emerged as a leading method for explicit likelihood estimation, offering advantages such as invertibility and gauge equivariance, which enable efficient global sampling [10, 13–18]. Furthermore, extensions of normalizing flows, including continuous normalizing flows [19–22] and stochastic normalizing flows [23–25], expand their capabilities in lattice simulations. However, in flow-based models, the training complexity increases significantly with larger lattice sizes [26–29]. Moreover, the use of the Kullback-Leibler divergence as the optimization objective can lead to mode collapse [30, 31], where the learned distribution fails to capture the full complexity of the target distribution. These challenges underscore the need to explore alternative generative models to further enhance sampling efficiency and reliability.

Recently, diffusion models (DMs) have gained significant attention for their success in generating high-quality samples across diverse domains [32–37], including applications in high-energy physics [38–41]. Diffusion models iteratively denoise random noise into realistic configurations through probabilistic steps [42]. Their application to lattice field theory was pioneered in Refs. [43, 44] for scalar fields, establishing the connection with stochastic quantization [45–48]. Subsequent studies introduced a Feynman path integral formulation [49] and analysed higher-order cumulants [50], further solidifying the theoretical foundation of diffusion models in this context. An application to data generated using complex Langevin dynamics can be found in Ref. [51]. In this work, we propose a novel framework based on diffusion models to address challenges in lattice gauge theory simulations [52]. To validate our approach, we conduct experiments in two-dimensional U(1) gauge theory, demonstrating that our model effectively samples topological quantities across varying coupling constants and lattice sizes without requiring additional training.

The paper is organized as follows. In Section 2 we discuss the issue of topological freezing, with subsections covering the Hybrid Monte Carlo (HMC) approach and topological charge. Section 3 introduces diffusion models and their training objectives, including the noise conditional score network and the U-Net architecture. In Section 4, we present our physics-conditioned sampler, which integrates the diffusion model with the notion of stochastic quantization and Langevin dynamics for conditional sampling while ensuring exactness. Section 5 details our numerical experiments, including data preparation, model setups, and evaluations across various lattice sizes and coupling constants. Section 6 concludes. More details are discussed in the Appendices.

## 2 Simulation of Lattice Gauge Fields

Abelian gauge theories in two Euclidean dimensions represent quantum electrodynamics (QED) on a plane and provide simplified models for gauge field theories [13, 53–55], while retaining some of the essential features of nonabelian theories in four dimensions: fermion confinement [56] and separated topological sectors [54]. In the two-dimensional U(1) gauge theory, a gauge-invariant lattice action can be defined as

$$S = -\beta \sum_x \text{Re}(U_{x,\square}), \quad (2.1)$$

where the plaquette variable is

$$U_{x,\square} \equiv U_{x,\mu} U_{x+\hat{\mu},\nu} U_{x+\hat{\nu},\mu}^\dagger U_{x,\nu}^\dagger. \quad (2.2)$$

On an  $L \times L$  square lattice with periodic boundary conditions, a gauge field on lattice site  $x$  in the direction  $\mu$  is represented by a link variable  $U_{x,\mu} = e^{i\phi_{x,\mu}}$ , where  $\phi_{x,\mu}$  is the gauge angle for the link. The plaquette, or the  $1 \times 1$  Wilson loop ( $W_{1 \times 1}$ ), is a gauge-invariant observable. Here  $\beta$  is the inverse coupling that controls the gauge interaction strength and ensures consistency with the continuum limit (at large  $\beta$ ) in simulations [53].

### 2.1 Hybrid Monte Carlo

In lattice field theory, physical properties are estimated via the expectation value of observables  $\hat{O}$ , representing the statistical expectation over all configurations in the physics distribution. The HMC algorithm is widely used to sample configurations efficiently by introducing auxiliary momenta, and utilizing Hamiltonian dynamics [3, 4, 53, 57, 58]. This enables effective phase space exploration and reduces autocorrelations, overcoming inefficiencies of random walk-based methods.

In particular, HMC evolves the system using Hamiltonian dynamics combined with a Metropolis acceptance step. The Hamiltonian  $H$  consists of the gauge action  $S[\phi]$  and the kinetic term for the conjugate momenta  $\pi_\mu(x)$  as,

$$H = \frac{1}{2} \sum_{\mu,x} \pi_\mu^2(x) + S_E[\phi]. \quad (2.3)$$

One initializes the gauge fields  $U_\mu(x)$ , using the angles  $\phi_{x,\mu}$  as degrees of freedom, randomly. For each gauge link, the conjugate momentum  $\pi_\mu(x)$  is drawn from a Gaussian distribution. The gauge links and momenta are then evolved according to classical equation of motion obtained from Eq. (2.3). These equations are discretized using a leapfrog integrator and, after a predefined number of molecular dynamics steps, we calculate the new Hamiltonian  $H'$  and apply the acceptance criterion,  $P_{\text{accept}} = \min(1, \exp\{H - H'\})$ . After generating a series of configurations, observables like Wilson loops or the topological charge are estimated by averaging over the ensemble of configurations.

## 2.2 Topological Charge Freezing

In gauge theories, the topological charge plays a key role in phenomena like confinement [54]. It is quantized, characterizing different vacuum states, and is linked to flux quantization and instantons [54]. The Atiyah-Singer Index Theorem [59] states that  $Q$  must be an integer and remain unchanged under continuous field transformations. Thus, topological charges reside in distinct sectors separated by energy barriers [9, 60].

In the two-dimensional case, the topological charge  $Q$  indicates the winding number of the gauge field configuration and on the lattice is given by

$$Q = \sum_x q(x) = \frac{1}{2\pi} \sum_x \arg U_{12}(x), \quad (2.4)$$

where the phase of the plaquette is chosen within the principal interval, i.e.,  $\in (-\pi, \pi]$ . The fluctuation of topological charge is described by the topological susceptibility,  $\chi_Q = \langle Q^2 \rangle / V$ , where  $V = L^2$  is the two-dimensional volume.

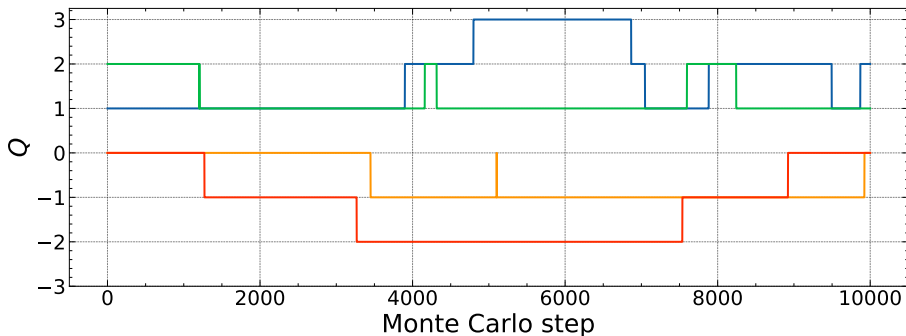


**Figure 1.** Monte Carlo evolution of the topological charge  $Q$  on multi-Markov chains after thermalization with  $L = 16$  and  $\beta = 7$ .

*Topological freezing* refers to the phenomenon where the topological charge  $Q$  remains constant over long Monte Carlo trajectories, preventing adequate sampling of different topological sectors [13, 61]. This issue may arise as a general feature in Monte Carlo simulations of lattice theories with non-trivial topological properties [9, 62–65]. It is referred to the critical slowing down of topological modes, where the autocorrelation time  $\tau_Q$  grows exponentially with the correlation length  $\xi_c$  as  $\tau_Q \sim \exp(c\xi_c)$ . Since  $\xi_c$  is inversely related

to the square root of the string tension,  $\xi_c \sim \sigma_s^{-1/2}$ , it diverges as the lattice spacing  $a$  decreases (or equivalently, as  $\beta$  increases), approaching the continuum limit [66]. Consequently, transitions between topological sectors become exponentially rare.

As illustrated in Fig. 1, see also Figs. 1 of Refs. [13, 61], samples within the same Markov chain (with different chains represented by different colors) remain confined to a limited number of topological sectors. This significantly hinders simulation efficiency and the accuracy of physical observables related to topology. In HMC, when the system is trapped in a restricted region of configuration space, transitions between isolated topological sectors are further suppressed [62, 67]. At large  $\beta$ , the action landscape may develop deep, narrow wells corresponding to these separated sectors, but Markov chains, which typically evolve by making small updates to state variables, struggle to transition between them [9, 68]. To address this challenge, improvements to existing algorithms or alternative approaches are necessary.

### 3 Diffusion Model and Score Matching

#### 3.1 Diffusion Models

Diffusion models generate samples by reversing the process of adding noise, with the goal of recovering the original distribution from pure noise [42]. While theoretically possible if the forward stochastic dynamics are known, in practice it is often difficult to determine the reverse process. To solve this problem, a deep model approximates the gradient of the logarithm of the data distribution, which feeds directly in the denoising process. The well-trained deep model on prepared lattice field configurations can serve as an effective drift term to generate more field configurations by evolving a stochastic differential equation [43]. It can provide an efficient and global sampler to simulate lattice quantum field theories [43, 44, 50, 69].

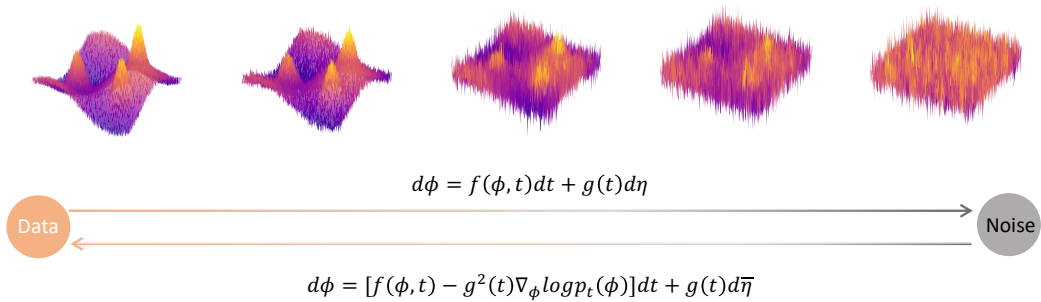


**Figure 2.** The forward diffusion process gradually adds noise and the reverse denoising process tries to remove noise. The two stochastic processes are described by two stochastic differential equations. The target distribution is typically unknown but its log derivative is learned from the training data.

As Fig. 2 demonstrates, in the limit of continuous time, the forward process, during which noise is added, follows a stochastic differential equation (SDE),

$$\frac{d\phi}{d\xi} = f(\phi, \xi) + g(\xi)\eta(\xi), \quad (3.1)$$

where the Langevin time  $\xi$  goes from 0 to  $T \equiv 1$ ,  $\eta$  is the noise term, satisfying  $\langle \eta(\xi)\eta(\xi') \rangle = \delta(\xi - \xi')$ , and  $f(\phi, \xi)$  is the drift term. The square of  $g(\xi)$  is the time-dependent scalar *diffusion coefficient*. In our case, the forward drift term  $f(\phi, \xi)$  is set to zero and the variance-expanding scheme is chosen, see, e.g., Ref. [70], with  $g(\xi) = \sigma^\xi$ . This way, the transition kernel in the forward process remains Gaussian, due to the additivity of Gaussian white noise,

$$p_\xi(\phi_\xi|\phi_0) = \mathcal{N}\left(\phi_\xi; \phi_0, \sigma_\xi \mathbf{I}\right), \quad \sigma_\xi = \frac{1}{\log \sigma^2}(\sigma^{2\xi} - 1). \quad (3.2)$$

In this setup, we can add noise at any  $0 < \xi \leq T$ , to achieve arbitrarily perturbed data.

The reverse denoising process corresponding to Eq. (3.1) is accomplished by a reverse SDE, representing an evolution backwards in time [71],

$$\frac{d\phi}{dt} = [f(\phi, t) - g^2(t)\nabla_\phi \log p_t(\phi)] + g(t)\bar{\eta}(t), \quad (3.3)$$

where the reverse time  $t$  runs from  $T$  to 0 and  $\bar{\eta}$  is a noise term in the reverse time direction, still satisfying  $\langle \bar{\eta}(t)\bar{\eta}(t') \rangle = \delta(t - t')$ . Importantly, the drift term in Eq. (3.3) includes the gradient of the logarithm of  $p_t(\phi)$ , the probabilistic distribution at time  $t$  in the forward diffusion process.

### 3.2 Noise Conditional Score Networks

Typically, the gradients  $\nabla_\phi \log p_t(\phi)$  in Eq. (3.3) are unknown. However, one can model a score function,  $s(\phi, \xi)$ , to match the gradients [70]. Due to demands of the scalability and ability to efficiently handle high-dimensional parameter spaces, we employ a deep neural network to model the score function. To further improve sampling efficiency, we introduce a noise scheme for the forward process, in which  $\xi_i$  ( $i = 1, \dots, N_T$ ) is a positive geometric sequence that satisfies  $\xi_1/\xi_2 = \dots = \xi_{N_T-1}/\xi_{N_T} > 1$ .

Consequently, we aim to train a conditional neural network to estimate the score of perturbed field configurations distribution, i.e.,

$$\forall \xi \in \{\xi_i\}_{i=1}^{N_T} : \quad s_\theta(\phi, \xi) \approx \nabla_\phi \log p_\xi(\phi_\xi|\phi_0), \quad (3.4)$$

as defined in Eq. (3.2). Here  $\theta$  denotes the parameters of the neural network. In training, we add known random noise to the data and train the network to estimate the noise scale. For a given  $\xi$ , the denoising *score matching* objective is to minimize the loss function,

$$\ell(\theta; \xi) \triangleq \frac{1}{2} \mathbb{E}_{p_{\text{data}}(\phi)} \mathbb{E}_{\tilde{\phi} \sim \mathcal{N}(\phi, \sigma_\xi^2 \mathbf{I})} \left[ \left\| s_\theta(\tilde{\phi}, \xi) + \frac{\tilde{\phi} - \phi}{\sigma_\xi^2} \right\|_2^2 \right]. \quad (3.5)$$

This is combined for all  $\xi \in \{\xi_i\}_{i=1}^{N_T}$  to get one unified objective,

$$\mathcal{L}(\theta; \{\xi_i\}_{i=1}^{N_T}) \triangleq \frac{1}{N_T} \sum_{i=1}^{N_T} \lambda(\xi_i) \ell(\theta; \xi_i), \quad (3.6)$$

where  $\lambda(\xi) = \sigma_\xi^2$  [70]. Under this choice, we have

$$\lambda(\xi) \ell(\theta; \xi) = \frac{1}{2} \mathbb{E} \left[ \left\| \sigma_\xi s_\theta(\tilde{\phi}, \xi) + \frac{\tilde{\phi} - \phi}{\sigma_\xi} \right\|_2^2 \right]. \quad (3.7)$$

Since  $(\tilde{\phi} - \phi)/\sigma_\xi \sim \mathcal{N}(0, I)$  and  $\|\sigma_\xi s_\theta(\phi, \xi)\|_2 \propto 1$ , we can deduce that the order of magnitude of  $\lambda(\xi) \ell(\theta; \xi)$  is independent of  $\xi$ .

With regard to the specific network architecture, similar as in Ref. [43], we adopt a U-Net architecture as shown in Fig. 3 to model the score function. It employs an encoder-decoder structure with symmetric skip connections. The receptive field grows as the network deepens, but each convolution acts locally, making it adaptable to arbitrarily large input sizes.

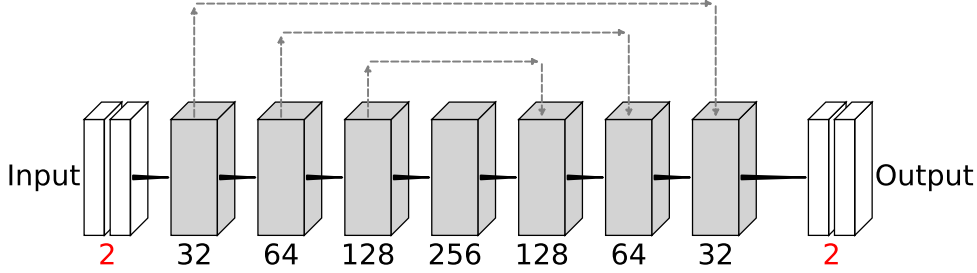


**Figure 3.** U-Net architecture. The gray lines with arrows denote skip connections between the encoding and decoding paths. In this study, the default input shape is specified as  $(\cdot, 2, 16, 16)$ , where the first dimension represents the batch size, the second corresponds to the channel dimension, and the last two denote the spatial dimensions of the field configuration.

**Input and Output:** The input tensor is defined as  $X \in \mathbb{R}^{N \times 2 \times L \times L}$ , where  $N$  denotes the batch size, 2 represents the two gauge link channels, and  $L$  (default 16) is the spatial lattice size. The output tensor  $Y$  has the same shape and approximates the score function,  $s_\theta(\phi, \xi)$ . For sampling, the lattice size  $L$  can be adjusted accordingly.

**U-Net Architecture:** The encoder applies convolutional layers,

$$h^{(l+1)} = \sigma(W^{(l)} * h^{(l)} + b^{(l)}). \quad (3.8)$$

Each layer follows group normalization,  $\hat{h}^{(l)} = (h^{(l)} - \mu_G) / \sqrt{\sigma_G^2 + \epsilon}$ . The decoder utilizes transposed convolutions,

$$h^{(l-1)} = \sigma(W_T^{(l-1)} \otimes h^{(l)} + b^{(l-1)}), \quad (3.9)$$

where  $\otimes$  denotes the deconvolution operation, which increases the spatial dimensions of the feature map. The decoder also employs skip connections,

$$\tilde{h}^{(l-1)} = \text{concat}(E^{(l-1)}, h^{(l-1)}), \quad (3.10)$$

where  $E^{(l-1)}$  indicates the corresponding encoder layer. Finally, the network output is normalized by the standard deviation of the perturbation kernel.

**Locality and Periodic Padding:** The lattice gauge action is constructed from Wilson loops, ensuring local interactions. Accordingly, the fully convolutional network (FCN) computes outputs locally, as

$$Y_{i,j} = f\left(\{X_{m,n} \mid m \in \mathcal{N}(i), n \in \mathcal{N}(j)\}\right). \quad (3.11)$$

It denotes the collection (or local patch) of input values that lie within a neighbourhood  $\mathcal{N}(i)$  around index  $i$  and  $\mathcal{N}(j)$  around index  $j$ . Periodic boundary conditions are enforced by using periodic padding, meaning that if an index exceeds the lattice boundaries, it wraps around according to the modulo operation.

## 4 Physics-Conditioned Sampler

Sampling in diffusion models can be realized [43] as a variant of stochastic quantization [45], an approach for quantizing field theories that is particularly useful for gauge theories [46, 47]. In stochastic quantization, one introduces a fictitious time  $\tau$ , extending a field  $\phi(x)$  to  $\phi(x, \tau)$ , which then evolves according to a Langevin equation,

$$\frac{\partial \phi(x, \tau)}{\partial \tau} = -\frac{\delta S[\phi]}{\delta \phi(x, \tau)} + \sqrt{2}\eta(x, \tau), \quad (4.1)$$

where  $\eta(x, \tau)$  is a Gaussian white noise. After a sufficient number of Langevin steps, the system reaches equilibrium with a distribution  $p(\phi) \propto e^{-S[\phi]}$ . This formulation effectively transforms the path integral measure of the quantum field theory into a stationary distribution of a stochastic process.

In our case, diffusion models generate samples via a similar stochastic differential equation derived from the variance-expanding version of Eq. (3.3),

$$\frac{\partial \phi(x, t)}{\partial t} = -g^2(t)s_{\delta}(\phi(x, t), t) + g(t)\eta(x, t), \quad (4.2)$$

starting from a Gaussian prior for  $\phi(x)$ . By gradually decreasing  $t$  from  $T = 1$  to 0 (where the noise vanishes), the resulting sample distribution becomes consistent with the target distribution used for training.

### 4.1 Physics-Conditioned Score Function

In this study, our target is to sample configurations at different values of the coupling  $\beta$  using a diffusion model trained at a single specific coupling  $\beta_0$ , without requiring additional training. To achieve this, we construct a *physics-conditioned sampler* by drawing

upon principles from statistical field theory. Configurations are sampled from the physical distribution,  $p(\phi) = \exp[-S(\phi; \beta)]/Z$ , where  $\beta$  is a parameter (the inverse coupling in our case). If the action is separable as  $S(\phi; \beta) = \beta \tilde{S}(\phi)$ , one may perform simulations at a reference value  $\beta_0$  and then use Ferrenberg-Swendsen or histogram reweighting [72] to obtain results for other values of  $\beta$ , provided the sampled ensembles have sufficient overlap. This idea has been proposed and validated for other field systems with different generative models [73, 74].

In diffusion models, the network-based score function  $s_\theta$  is trained to approximate the drift term  $\nabla_\phi \log p_t(\phi)$  in the reverse diffusion process. In contrast, in Langevin simulations of fields, the drift term is given by the functional derivative of the action,  $-\delta S[\phi]/\delta\phi(x, \tau)$ . If the diffusion model is well-trained, when the noise scale reaches 0, the score function should approximate the actual drift term,  $s_{\hat{\theta}}(\phi(x, 0), 0; \beta) \simeq -\delta S(\phi; \beta)/\delta\phi(x)$ . For separable actions, such as in pure gauge theories, both the action and its derivative scale linearly with the coupling  $\beta$ . This suggests that a well-trained score network at a reference coupling  $\beta_0$  can directly replace the drift term in Langevin simulations at arbitrary  $\beta$  when equilibrium is reached around the final steps. Then one can generate configurations at different values of  $\beta$  from the trained diffusion model directly, using the sampler to be introduced in the next section.

## 4.2 Metropolis-Adjusted Annealed Langevin Algorithm

As explained earlier, generating samples for U(1) lattice gauge theory at different coupling values is only feasible if equilibrium is achieved in the final noise-scale steps. To ensure this, we use the *annealed Langevin scheme* proposed in Ref. [34]. In Fig. 4, the reverse denoising process is demonstrated along the horizontal time axis, with different noise-scales at different  $t$ . Each orange double arrow can be expanded into a dashed orange box describing the annealed scheme. This is where we run evolution along another time direction,  $0 < \tau \leq T_A$ , with the fixed drift term  $-\frac{\beta}{\beta_0} g^2(t) s_{\hat{\theta}}(\phi_t, t)$ . The final state of the annealed Langevin evolution is copied as the initial state at the next noise scale. By performing multiple Langevin updates at each progressively decreasing noise scale  $t_i$ , one ensures that the distribution approaches  $p(\phi, t_i) \propto e^{-S_{DM}(\phi, t_i)}$ , where  $\partial S_{DM}(\phi, t_i)/\partial\phi = -\frac{\beta}{\beta_0} \hat{s}_\theta(\phi, t_i)$ . This will eventually bring us to  $S_{DM}(\phi, t_i \rightarrow 0) \simeq S(\phi; \beta)$  in the final steps. The detailed set-up of the annealed scheme can be found in Appendix A.

In addition, to ensure that a Markov chain has the correct stationary measure, one can add a Metropolis-Hastings filter, i.e., an accept-reject step, along it. We extended the Metropolis-adjusted Langevin algorithm (MALA) [75, 76] for the annealed process to update configurations and build multi-Markov chains during the final steps,  $0 \leq t \leq 0.01$ .<sup>1</sup> This will prepare  $N_C$  chains for collecting configurations to estimate observables accurately. As shown in the dashed blue box of Fig. 4, the Metropolis-adjusted procedure is employed in the annealed process for the last  $N_C$  noise-scales. Since  $S_{DM}(\phi, t_i \rightarrow 0) \simeq S(\phi; \beta)$ , the sampler can reach a reasonably high acceptance rate as shown in Appendix B.

<sup>1</sup>In our case,  $t \leq 0.01$  means  $N_C = 55$  discrete time steps along the diffusion model backward direction in the set-up of noising scheme, using  $0.9^{N_T - N_C} \leq 0.01$ . More details can be found in Appendix A.

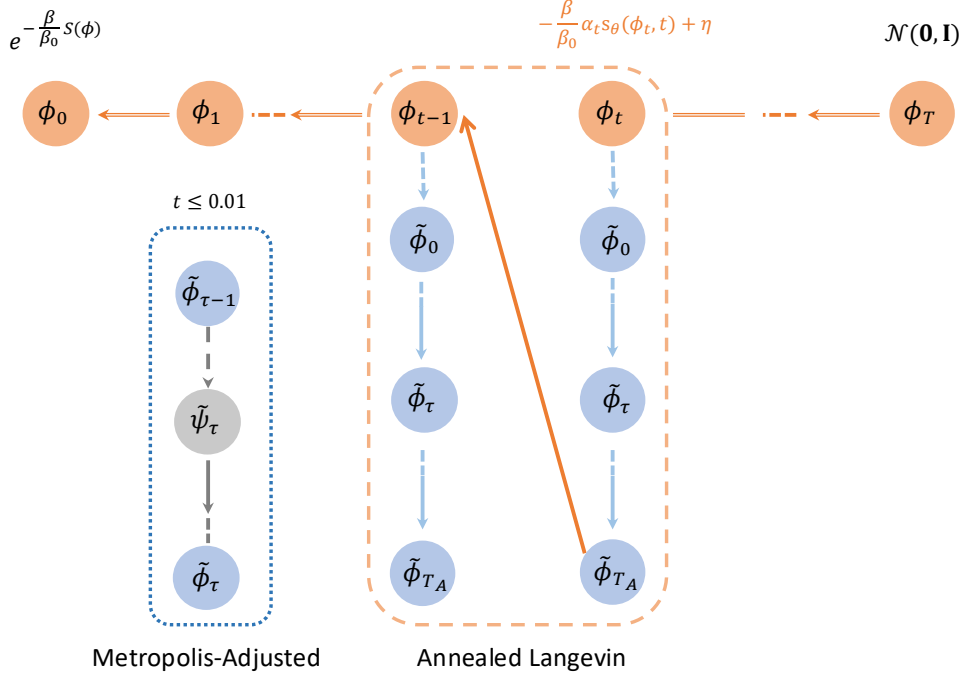


**Figure 4. Metropolis-adjusted annealed Langevin sampler.** The evolution along the horizontal axis represents the diffusion model running backwards in time  $t$  from the naive distribution  $\mathcal{N}(\mathbf{0}, \mathbf{I})$  to the target physical distribution. The evolution along the vertical axis corresponds to the annealed Langevin dynamics with time  $\tau$  and a fixed drift term, where the first dashed arrows indicate the copy operation. To distinguish them, we use a different notation to label the field variables.

In a general MALA [75, 76], from the current state  $\phi_\tau$ , the proposed update is

$$\psi_{\tau+1} = \phi_\tau + \alpha_i f(\phi_\tau, \tau) + \sqrt{2\alpha_i} \eta, \quad (4.3)$$

where  $\alpha_i$  is a redefined noise-scale parameter which can be found in Appendix A. The accept-reject step is

$$\phi_{\tau+1} = \begin{cases} \psi_{\tau+1} & \text{with probability } \min \left\{ 1, \frac{p(\psi_{\tau+1})q(\phi_\tau|\psi_{\tau+1})}{p(\phi_\tau)q(\psi_{\tau+1}|\phi_\tau)} \right\}, \\ \phi_\tau & \text{with the remaining probability,} \end{cases} \quad (4.4)$$

where  $p(\phi)$  is computed from the known physical distribution. Note that conditioned on  $\phi_\tau$ , the proposal step boils down to drawing a Gaussian with mean  $\phi_\tau + \alpha_i f(\phi_\tau, \tau)$  and variance  $\sqrt{2\alpha_i} I_\tau$ . Hence, the proposal kernel has the explicit form

$$q(\phi_\tau|\psi_{\tau+1}) = \frac{1}{(4\pi\alpha_i)^{n/2}} \exp \left( -\frac{1}{4\alpha_i} \|\phi_\tau - (\psi_{\tau+1} + \alpha_i f(\psi_{\tau+1}, \tau + 1))\|_2^2 \right), \quad (4.5)$$

where  $n$  is the number of degrees of freedom, which is  $n = V$  in our case. The transition probability can then be computed explicitly, as

$$\frac{p(\psi_{\tau+1})q(\phi_\tau|\psi_{\tau+1})}{p(\phi_\tau)q(\psi_{\tau+1}|\phi_\tau)} = \exp\left(-S(\psi_{\tau+1}) - \frac{1}{4\alpha_i}\|\phi_\tau - (\psi_{\tau+1} + \alpha_i f(\psi_{\tau+1}, \tau + 1))\|_2^2 + S(\phi_\tau) + \frac{1}{4\alpha_i}\|\psi_{\tau+1} - (\phi_\tau + \alpha_i f(\phi_\tau, \tau))\|_2^2\right). \quad (4.6)$$

Combined with the annealed scheme, the Metropolis-adjusted annealed Langevin algorithm can generate exact configurations at different inverse couplings  $\beta$ . A detailed set-up can be found in Algorithm 2 of Appendix A. In fact, the classical Langevin simulation is obtained by replacing the time-dependent score function by the physical drift term derived from the given action. We will compare our results with the Langevin simulation according to Eq. (4.1). In this study, the results of the diffusion model are all generated by the Metropolis-adjusted Langevin annealed algorithm.

## 5 Numerical Experiments

For building a training data set, we generated 30720 configurations at  $\beta = 1.0$  on a  $16 \times 16$  lattice. For testing, we generated 1024 configurations at  $\beta = 1.0, 3.0, 5.0, 7.0, 9.0, 11.0$  on different lattices of size  $8 \times 8$ ,  $16 \times 16$  and  $32 \times 32$ . The gauge symmetry of the theory is employed for data augmentation, where a set of configurations resulting from a gauge transformation is treated as a new set of configurations. This informs our neural network that, despite numerical differences, the underlying physical properties remain the same after gauge transformations.

In this work, configurations for training are generated by HMC, which is an efficient method for generating gauge field configurations at least at  $\beta = 1.0$ . To generate better samples, for each Markov chain in HMC, we have a “200-step burn-in loop” for thermalization, and after 128 additional steps, we select the final step of the 128-step update as a configuration. Here one step indicates one MC trajectory with a well-established HMC integrator, as in Ref. [43].

### 5.1 Performance in the Unfrozen Region

#### 5.1.1 Training and validation

First, we evaluate the training performance in the topologically unfrozen region at  $\beta = 1$ . All configurations are generated by the original sampler, as introduced in Ref. [43], from the trained diffusion model. In Fig. 5, the distributions of the Wilson loop (left) and the topological charge (right) are shown as orange bins, demonstrating consistency with the HMC results, which are represented by blue envelopes and bins. Qualitatively, the diffusion model achieves comparable performance to HMC in estimating both local and topological observables in the topologically unfrozen region. More quantitative results are shown in the following sections with our new sampler.

#### 5.1.2 Generation at different lattice sizes

As a further validation and direct extrapolation, the performance across different lattice sizes is evaluated, see Table 1. These results demonstrate that the estimates of the Wilson

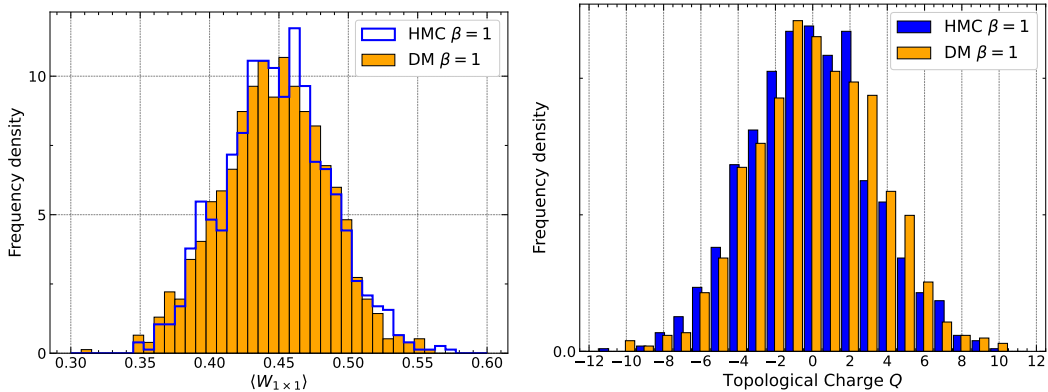


**Figure 5.** Histograms of the Wilson loop (left) and the topological charge (right) at  $\beta = 1$ ,  $L = 16$  from the testing data-set (HMC) and from the trained diffusion model (DM).

loop (left) remain consistent across all lattice sizes, agreeing with the analytical result, see Appendix C. Similarly, the calculation of the topological charge (right) in Table 1 exhibits stability, indicating that the DM accurately captures the underlying physics. The number of independent configurations is 1024 in all cases. Since the DM was trained on a  $16 \times 16$  lattice only, these findings highlight the capability of DMs to train on small volumes and generalize to larger volumes without loss of accuracy, owing to their fully convolutional architecture introduced in Section 3.2. This property significantly reduces memory requirements during training, making DMs a feasible approach for directly generating configurations in larger systems.

**Table 1.** Comparison of observables for  $\beta = 1$  at different lattice sizes

Lattice Size ( $L$ )	1 $\times$ 1 Wilson Loop				Topological Susceptibility			
	HMC	DM	Langevin	Exact	HMC	DM	Langevin	Exact
8	0.447(72)	0.445(74)	0.443(80)	0.446	0.0402(17)	0.0413(18)	0.0418(18)	0.0406
16	0.447(37)	0.446(37)	0.444(36)	0.446	0.0416(16)	0.0422(17)	0.0421(20)	0.0406
32	0.446(18)	0.445(19)	0.445(18)	0.446	0.0428(19)	0.0415(18)	0.0412(17)	0.0406
64	0.446(9)	0.446(11)	0.445(9)	0.446	0.0426(19)	0.0427(20)	0.0420(19)	0.0406

## 5.2 Generation in the Frozen Region

### 5.2.1 Mitigate freezing

Next, we evaluate the model’s performance at different coupling values, without additional training, in the topologically frozen region using the physics-conditioned sampler introduced in Section 4.2.

Using the same trained diffusion model, we generate 1024 configurations at  $\beta = 7$  and compare them with a set of 1024 configurations generated via HMC. The results are presented in Fig. 6. We observe that the Wilson loop distributions (left) remain consistent

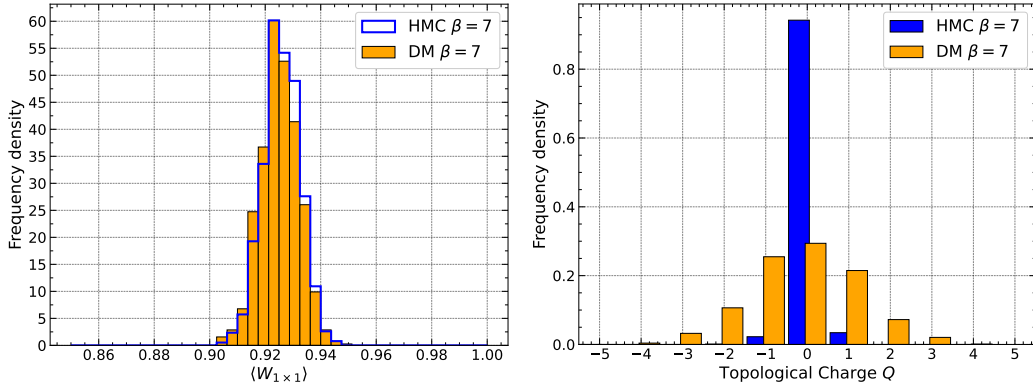


**Figure 6.** Comparison of distributions for the Wilson loop (left) and the topological charge (right) at  $\beta = 7$  from the testing data-set (HMC) and from the DM trained at  $\beta = 1$  but conditioned at  $\beta = 7$ . The number of independent configurations is 1024 in both cases.

**Table 2.** Comparison of the  $l \times l$  Wilson Loops for  $L = 16, \beta = 7$

Loop size ( $l$ )	HMC	DM	Langevin	Exact
1	0.926(7)	0.926(7)	0.924(6)	0.926
2	0.737(31)	0.737(32)	0.730(34)	0.734
3	0.510(67)	0.496(72)	0.489(73)	0.498
4	0.311(97)	0.283(96)	0.283(106)	0.290

between the two approaches. A more detailed comparison of Wilson loop at different sizes is provided in Table 2, which also includes a comparison with straightforward Langevin simulations. However, for the topological charge in Fig. 6 (right), HMC exhibits topological freezing, sampling only values of the topological charge  $Q$  near or at zero. In contrast, the physics-conditioned sampler using the DM explores a broader range of topological sectors, leading to a larger topological susceptibility that is consistent with the analytical results. In addition, one can also estimate the likelihood for different conditions to evaluate whether the model is approaching the target physics distribution, which is discussed in Appendix D.

### 5.2.2 Generation at different lattice sizes and couplings

Next we estimate observables at both different couplings and lattice sizes. Table 3 presents a comparison of observables at fixed coupling  $\beta = 7$  for lattice sizes  $L = 8 \times 8, 16 \times 16$  and  $32 \times 32$ . The observables studied are the  $1 \times 1$  Wilson loop and the topological susceptibility. For the three samplers, the Wilson loop values remain relatively stable across different lattice sizes and numerical methods, with all deviations within statistical uncertainties. However, the topological susceptibility shows significant variation depending on the method used. In particular, Langevin dynamics yields notably higher susceptibility values compared to the exact results, while the HMC results indicate freezing. The DM remains closer to the exact predictions.

**Table 3.** Comparison of observables for  $\beta = 7$  at different lattice sizes

Lattice Size ( $L$ )	$1 \times 1$ Wilson Loop				Topological Susceptibility			
	HMC	DM	Langevin	Exact	HMC	DM	Langevin	Exact
8	0.927(13)	0.926(13)	0.921(13)	0.926	0.00006(3)	0.0040(12)	0.0143(5)	0.0040
16	0.926(7)	0.926(7)	0.924(6)	0.926	0.00013(2)	0.0043(5)	0.0131(5)	0.0039
32	0.926(3)	0.925(4)	0.924(4)	0.926	0.00013(2)	0.0040(4)	0.0137(6)	0.0039

**Table 4.** Comparison of observables for  $L = 16$  at different couplings

coupling ( $\beta$ )	$1 \times 1$ Wilson Loop				Topological Susceptibility			
	HMC	DM	Langevin	Exact	HMC	DM	Langevin	Exact
3	0.811(17)	0.811(17)	0.809(17)	0.810	0.0096(4)	0.0114(6)	0.0106(14)	0.0111
5	0.894(9)	0.894(9)	0.891(10)	0.894	0.0048(2)	0.0058(5)	0.0075(3)	0.0057
7	0.926(7)	0.926(7)	0.924(6)	0.926	0.00013(2)	0.0045(5)	0.0131(5)	0.0039
9	0.944(3)	0.942(4)	0.940(6)	0.942	0	0.0031(4)	0.0154(7)	0.0029
11	0.954(3)	0.953(4)	0.950(5)	0.953	0	0.0025(3)	0.0165(13)	0.0024

Table 4 examines the dependence of observables on the coupling constant, at a fixed lattice size of  $16 \times 16$ . As  $\beta$  increases, the Wilson loop approaches 1, with reduced fluctuations. Similarly, the topological susceptibility decreases with increasing  $\beta$ , indicating a suppression of topological fluctuations at weak coupling.

While the diffusion model maintains close agreement with the exact values, the HMC results exhibit again topological freezing, and the Langevin method systematically overestimates the susceptibility, particularly at higher  $\beta$ . These findings underscore the effectiveness of physics-conditioned diffusion models in computing lattice gauge theory observables.

## 6 Summary and Outlook

In this study, we applied diffusion models to generate gauge field configurations. The correspondence between the stochastic differential equations encountered in diffusion models and in stochastic quantization enables the model to generate configurations at different lattice sizes and coupling constants without additional retraining. To ensure that the sampled distribution corresponds to the physical distribution, we combined the Metropolis-adjusted Langevin algorithm with the annealed Langevin sampler. Our results demonstrate that this multi-chain sampler effectively mitigates topological freezing at large  $\beta$ , and that the diffusion model proposes improved configurations for the Markov chains, leading to estimates of observables that remain consistent with exact results.

In our study, the diffusion model performs well for Abelian pure gauge fields, even with a simple U-net architecture. Extending this approach to non-Abelian gauge theories, including fermionic systems, appears straightforward; however, the non-locality of fermion determinants remains a significant challenge. The first attempt for a complex action (sign) problem has been reported recently [51]. The integration of diffusion models with neural

networks specifically designed for lattice configurations [77–80] is also a promising direction. The scalability of diffusion models suggests its potential for generating configurations on larger lattices at large  $\beta$ , requiring training only on samples from smaller lattice sizes and lower  $\beta$  values. Our objective for the future is to develop a complementary approach that enhances the efficiency and accuracy of lattice Quantum Chromodynamics computations, particularly in regimes where traditional techniques face limitations.

## Acknowledgments

We thank Shiyang Chen and Diao E. Habibi for comments and Drs. Akinori Tanaka, Tetsuo Hatsuda, Andreas Ipp, Gurtej Kanwar, Fernando Romero-López, and Shuzhe Shi for helpful discussions. We thank the DEEP-IN working group at RIKEN-iTHEMS for support in the preparation of this paper. WW and QZ are supported in part by Natural Science Foundation of China under grants No. 12125503 and 12335003, and SJTU Kunpeng & Ascend Center of Excellence. GA is supported by STFC Consolidated Grant ST/X000648/1. KZ is supported by the CUHK-Shenzhen university development fund under grant No. UDF01003041 and UDF03003041, and Shenzhen Peacock fund under No. 2023TC0179. LW is also supported by the RIKEN TRIP initiative (RIKEN Quantum) and JST-BOOST grant.

**Research Data and Code Access** – The code and data used for this manuscript can be found at <https://github.com/zzzqt/DM4U1>.

**Open Access Statement** – For the purpose of open access, the authors have applied a Creative Commons Attribution (CC BY) licence to any Author Accepted Manuscript version arising.

## A Langevin Sampler

---

### Algorithm 1 Annealed Langevin Sampler

---

**Require:**  $\{t_i\}_{i=1}^{N_T}, \epsilon, N_A$

- 1: Initialize  $\phi_0$
  - 2: **for**  $i \leftarrow 1$  to  $N_T$  **do**
  - 3:    $\alpha_i \leftarrow \epsilon \cdot g \cdot t_i^2 / t_{N_T}^2$   $\triangleright \alpha_i$  is the step size.
  - 4:    $\tilde{\phi}_0 \leftarrow \phi_{i-1}$
  - 5:   **for**  $\tau \leftarrow 1$  to  $N_A$  **do**
  - 6:     Draw  $\eta \sim \mathcal{N}(0, I)$
  - 7:      $\tilde{\phi}_\tau \leftarrow \tilde{\phi}_{\tau-1} + \frac{\beta}{\beta_0} \alpha_i s_\theta(\tilde{\phi}_{\tau-1}, t_i) + \sqrt{2\alpha_i} \eta$
  - 8:   **end for**
  - 9:    $\phi_i \leftarrow \tilde{\phi}_{N_A}$
  - 10: **end for**
  - 11: **return**  $\phi_{N_T}$
- 

---

### Algorithm 2 Metropolis-Adjusted Annealed Langevin Sampler

---

**Require:**  $\{t_i\}_{i=1}^{N_T}, \epsilon, N_A$

- 1: Initialize  $\phi_0$
  - 2: **for**  $i \leftarrow 1$  to  $N_T$  **do**
  - 3:    $\alpha_i \leftarrow \epsilon \cdot g \cdot t_i^2 / t_{N_T}^2$   $\triangleright \alpha_i$  is the step size.
  - 4:    $\tilde{\phi}_0 \leftarrow \phi_{i-1}$
  - 5:   **for**  $\tau \leftarrow 1$  to  $N_A$  **do**
  - 6:     Draw  $\eta \sim \mathcal{N}(0, I)$
  - 7:     Propose  $\tilde{\psi}_\tau = \tilde{\phi}_{\tau-1} + \frac{\beta}{\beta_0} \alpha_i s_\theta(\tilde{\phi}_{\tau-1}, t_i) + \sqrt{2\alpha_i} \eta$
  - 8:     **if**  $t_i < 0.01$  **then**
  - 9:        $P_i \leftarrow \min \left\{ 1, \frac{p(\tilde{\psi}_{\tau+1})q(\tilde{\phi}_\tau | \tilde{\psi}_{\tau+1})}{p(\tilde{\phi}_\tau)q(\tilde{\psi}_{\tau+1} | \tilde{\phi}_\tau)} \right\}$
  - 10:       Draw  $k \sim \text{Uniform}(0, 1)$
  - 11:       **if**  $k_i < P_i$  **then**
  - 12:           $\tilde{\phi}_\tau \leftarrow \tilde{\psi}_\tau$
  - 13:       **else**
  - 14:           $\tilde{\phi}_\tau \leftarrow \tilde{\phi}_{\tau-1}$
  - 15:       **end if**
  - 16:     **else**
  - 17:        $\tilde{\phi}_\tau \leftarrow \tilde{\psi}_\tau$
  - 18:     **end if**
  - 19:   **end for**
  - 20:    $\phi_i \leftarrow \tilde{\phi}_{N_A}$
  - 21: **end for**
  - 22: **return**  $\phi_{N_T}$
-

Algorithm 1 provides the pseudocode for our annealed Langevin scheme. Here  $g$  is the diffusion coefficient,  $t_i$  is chosen as a geometric series starting from 1 with a common ratio of 0.9 and a total of  $N_T = 100$  steps,  $\epsilon$  is fixed to  $5e^{-9}$  such that  $\epsilon \cdot t_0^2/t_{N_T}^2 \sim 1$ , and we set  $N_A = 1000$ . The initial distribution is taken to be the standard normal distribution. Algorithm 2 is the pseudocode of the integration of the Metropolis-adjusted Langevin algorithm with the annealed scheme. If no further explanation is given, all related settings are the same as for the Algorithm 1. The transition probability is computed from the given physical action and the learned score functions.

## B Autocorrelation Time

Although in our approach multiple Markov chains are employed to generate independent samples, the dynamics in a single chain can be compared with other Monte Carlo methods. For traditional Monte Carlo methods, the characteristic length of autocorrelations for any observable  $\mathcal{O}$  can be defined by the integrated autocorrelation time  $\tau_{\mathcal{O}}^{\text{int}}$  [81].

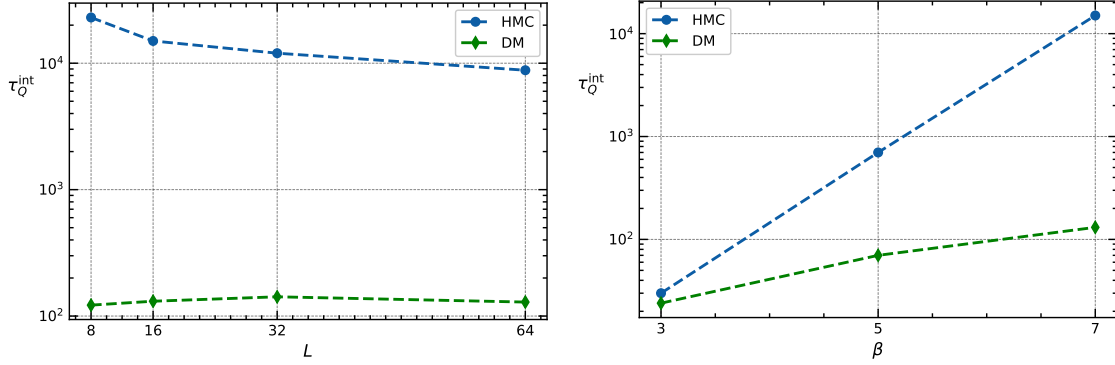


**Figure 7.** Comparison of integrated autocorrelation time in a single Markov chain for HMC and the DM at  $\beta = 7$  for different lattice sizes  $L$  (left), and at  $L = 16$  for different couplings  $\beta$  (right)

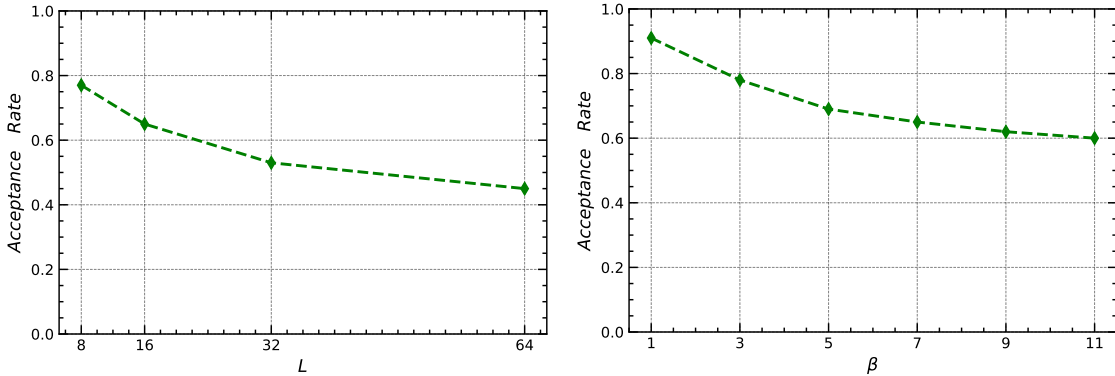


**Figure 8.** Dependence of acceptance rate in a single Markov chain of a DM at  $\beta = 7$  for different lattice sizes  $L$  (left), and at  $L = 16$  for different couplings  $\beta$  (right)

Fig. 7 compares the integrated autocorrelation time of the topological charge,  $\tau_Q^{\text{int}}$ , for HMC and DM. For both methods,  $\tau_Q^{\text{int}}$  increases as  $\beta$  is raised. In a single Markov chain within HMC, once equilibrium is reached, the topological charge rarely evolves at large  $\beta$ , whereas the diffusion model exhibits significantly better ergodicity. DM also demonstrates stability across different lattice sizes, with  $\tau_Q^{\text{int}} \approx 130$  for all sizes at  $\beta = 7$ . Additionally, we test a Metropolis-adjusted traditional Langevin sampler by replacing only the drift term in Algorithm 2 with  $-\delta S[\phi]/\delta\phi(x, \tau)$ , considering both single-chain and multi-chain settings. The results are unsatisfactory: for the single chain,  $\tau_Q^{\text{int}}$  remains significantly large even at small  $\beta$ , while for the multi-chain approach, the topological susceptibility is several times larger than the analytical result.

We also compute the dependence of the acceptance rate on lattice size and different coupling values. Fig. 8 shows that the acceptance rate does not decrease significantly as the lattice size and  $\beta$  increase.

## C Analytical Results

The action of the two-dimensional U(1) gauge field theory can be written as

$$S(U_\square) = -\beta \sum_{\square} \text{Re}(U_\square) = -\frac{\beta}{2} \sum_{\square} [U_\square + U_\square^{-1}]. \quad (\text{C.1})$$

The partition function is defined as

$$Z = \int dU_\square e^{-S(U_\square)} = \int \prod_{\square} dU e^{\frac{\beta}{2}[U+U^{-1}]} = \prod_{\square} \int \frac{d\phi}{2\pi} e^{\beta \cos \phi} = [I_0(\beta)]^V, \quad (\text{C.2})$$

where we used that the Haar measure with the defining representation [15],  $U = e^{-i\phi}$ , is  $d\phi/(2\pi)$ . The integral is the modified Bessel function of the first kind,  $I_{n=0}(\beta)$ .

The partition function in fixed topology can also be derived from the known partition function in the  $\theta$ -vacuum [8, 82, 83]. At sufficiently large volume ( $V \rightarrow \infty$ ),

$$\begin{aligned} Z_Q &= \int \frac{d\phi}{2\pi} e^{\beta \sum_{\square} \cos \phi} \delta\left(\sum_{\square} \frac{\phi}{2\pi} - Q\right) \\ &= \int_{-\infty}^{\infty} dk e^{-ikQ} \prod_{\square} I_{k/(2\pi)}(\beta) = \int_{-\pi}^{\pi} d\theta e^{-i\theta Q} [I_{\theta/(2\pi)}(\beta)]^V. \end{aligned} \quad (\text{C.3})$$

In the second line we changed variables, which makes the integrated function decays rapidly beyond the interval  $[-\pi, \pi]$ . From the partition function, one can derive the probability density over  $Q$ ,

$$p(Q) \equiv \frac{Z_Q}{Z} = \int_{-\pi}^{\pi} d\theta e^{-i\theta Q} \left[ \frac{I_{\theta/(2\pi)}(\beta)}{I_0(\beta)} \right]^V. \quad (\text{C.4})$$

The susceptibility of the topological charge,  $\chi_Q \equiv \langle Q^2 \rangle / V$ , is given by

$$\chi_Q = \frac{1}{V} \int dQ p(Q) Q^2, \quad (\text{C.5})$$

where  $Q$  varies over all integers. These expressions are consistent with Refs. [8, 82–84].

On  $L \times L$  lattices with periodic boundary conditions, the average value of the Wilson loops for  $U(1)$  gauge fields can be derived using integration over the set of plaquette variables after gauge fixing [15],

$$\langle W_A \rangle = \frac{1}{Z} \sum_k I_k(\beta)^{V-A} \left( \int dU_{\square} U^{k+1} e^{\frac{\beta}{2}[U+U^{-1}]} \right) = \frac{\sum_k I_k(\beta)^{V-A} I_{k+1}(\beta)^A}{\sum_k I_k(\beta)^V}, \quad (\text{C.6})$$

where  $A$  indicates the area of the plaquette variables.

## D Likelihood Estimation

Samplers based on stochastic differential equations incorporate a noise term, making it impossible to directly estimate the likelihood of generated samples. In contrast, the probability flow of an ordinary differential equation (ODE) [70] enables such likelihood estimation, as introduced in Ref. [43]. The ODE sampler is sufficient for generating configurations at  $\beta = 1$ . By comparing the log-likelihood of samples generated by the trained diffusion model with the physical action, we can assess whether the model has successfully captured the underlying physical distribution.

**ODE sampler and estimator.** To estimate the log-likelihood as if the samples are generated by the probability flow ODE, we use the RK45 ODE solver provided by `scipy.integrate.solve_ivp` with `atol=1e-6` and `rtol=1e-6`. To generate configurations at  $\beta$  and estimate the likelihood, the starting point  $\tilde{\phi}_0 \sim \mathcal{N}(0, \sigma_t^2 I)$  and the time interval starts from 1 and ends with 0. The ODE and log-likelihood are computed through

$$\frac{d}{dt} \begin{bmatrix} \phi(t) \\ \log p(\phi(t), t) \end{bmatrix} = \frac{1}{2} \begin{bmatrix} -g^2 \cdot s_{\theta}(\phi(t), t) \\ -\sum_{\phi} g^2 \cdot \frac{\partial s_{\theta}(\phi(t), t)}{\partial \phi} \end{bmatrix}. \quad (\text{D.1})$$

In Fig. 9 we show the correlation of the log-likelihood estimated by the DM, denoted by  $S_{\text{eff}} = -\log(q(\phi))$ , and the real action  $S(\phi)$ .

For  $\beta = 7$ , since the backward SDE has been modified due to the physics-conditioned design, there is no straightforward method to directly estimate the likelihood as described above. To address this, we trained a new model using 30,720 samples at  $\beta = 7$  generated by Algorithm 1 and applied the same data augmentation method as outlined in Sec. 5. Using this newly trained model and Eq. (D.1), we can evaluate the quality of samples generated by Algorithm 2. Fig. 10 illustrates the relationship between the log-likelihood and the physical action, treating the samples as if they were generated by the new model using the ODE sampler.

## References

- [1] U. Wolff, *CRITICAL SLOWING DOWN*, *Nucl. Phys. B Proc. Suppl.* **17** (1990) 93.
- [2] U. Wolff, *Collective Monte Carlo Updating for Spin Systems*, *Phys. Rev. Lett.* **62** (1989) 361.

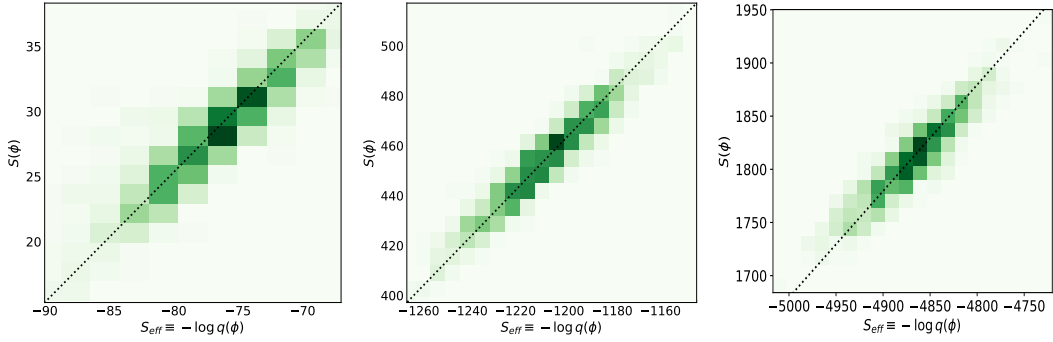


**Figure 9.** Likelihood of generated samples at  $L = 8$  (left),  $32$  (middle) and  $64$  (right). The vertical axis represents the true action of the configurations, while the horizontal axis corresponds to the log-likelihood generated by the diffusion model, obtained from the probability flow ODE.

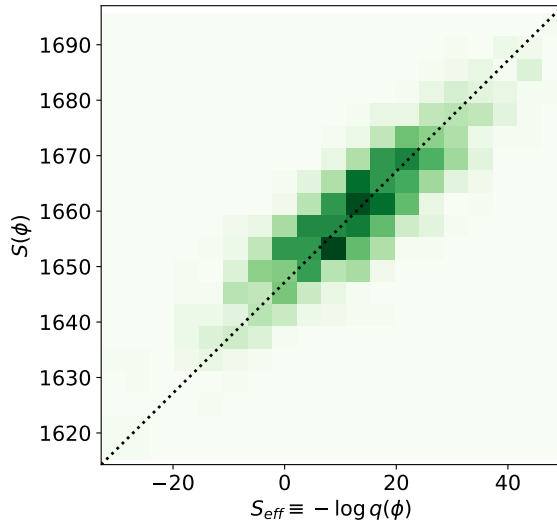


**Figure 10.** Likelihood of generated samples at  $L = 16, \beta = 7$ . The vertical axis represents the true action of the configurations, while the horizontal axis corresponds to the log-likelihood generated by the diffusion model, obtained from the probability flow ODE.

- [3] M. Hasenbusch, *Speeding up the hybrid Monte Carlo algorithm for dynamical fermions*, *Phys. Lett. B* **519** (2001) 177 [[hep-lat/0107019](#)].
- [4] M. Hasenbusch and K. Jansen, *Speeding up lattice QCD simulations with clover improved Wilson fermions*, *Nucl. Phys. B* **659** (2003) 299 [[hep-lat/0211042](#)].
- [5] N. Prokof'ev and B. Svistunov, *Worm Algorithms for Classical Statistical Models*, *Phys. Rev. Lett.* **87** (2001) 160601 [[cond-mat/0103146](#)].
- [6] J. Brannick, R.C. Brower, M.A. Clark, J.C. Osborn and C. Rebbi, *Adaptive Multigrid Algorithm for Lattice QCD*, *Phys. Rev. Lett.* **100** (2008) 041601 [[0707.4018](#)].
- [7] M.S. Albergo, G. Kanwar and P.E. Shanahan, *Flow-based generative models for Markov chain Monte Carlo in lattice field theory*, *Phys. Rev. D* **100** (2019) 034515 [[1904.12072](#)].

- [8] D. Albande, P. Hernández, A. Ramos and F. Romero-López, *Topological sampling through windings*, *Eur. Phys. J. C* **81** (2021) 873 [2106.14234].
- [9] T. Eichhorn, G. Fuwa, C. Hoelbling and L. Varnhorst, *Parallel tempered metadynamics: Overcoming potential barriers without surfing or tunneling*, *Phys. Rev. D* **109** (2024) 114504 [2307.04742].
- [10] K. Cranmer, G. Kanwar, S. Racanière, D.J. Rezende and P.E. Shanahan, *Advances in machine-learning-based sampling motivated by lattice quantum chromodynamics*, *Nature Rev. Phys.* **5** (2023) 526 [2309.01156].
- [11] K. Zhou, L. Wang, L.-G. Pang and S. Shi, *Exploring QCD matter in extreme conditions with Machine Learning*, *Prog. Part. Nucl. Phys.* **135** (2024) 104084 [2303.15136].
- [12] L. Wang, Y. Jiang, L. He and K. Zhou, *Continuous-Mixture Autoregressive Networks Learning the Kosterlitz-Thouless Transition*, *Chin. Phys. Lett.* **39** (2022) 120502 [2005.04857].
- [13] G. Kanwar, M.S. Albergó, D. Boyda, K. Cranmer, D.C. Hackett, S. Racanière et al., *Equivariant flow-based sampling for lattice gauge theory*, *Phys. Rev. Lett.* **125** (2020) 121601 [2003.06413].
- [14] D. Boyda, G. Kanwar, S. Racanière, D.J. Rezende, M.S. Albergó, K. Cranmer et al., *Sampling using  $SU(N)$  gauge equivariant flows*, *Phys. Rev. D* **103** (2021) 074504 [2008.05456].
- [15] G. Kanwar, *Machine Learning and Variational Algorithms for Lattice Field Theory*, Ph.D. thesis, MIT, 2021. 2106.01975.
- [16] M.S. Albergó, D. Boyda, D.C. Hackett, G. Kanwar, K. Cranmer, S. Racanière et al., *Introduction to Normalizing Flows for Lattice Field Theory*, 2101.08176.
- [17] G. Kanwar, *Flow-based sampling for lattice field theories*, *PoS LATTICE2023* (2024) 114 [2401.01297].
- [18] S. Chen, O. Savchuk, S. Zheng, B. Chen, H. Stoecker, L. Wang et al., *Fourier-flow model generating Feynman paths*, *Phys. Rev. D* **107** (2023) 056001 [2211.03470].
- [19] R.T.Q. Chen, Y. Rubanova, J. Bettencourt and D. Duvenaud, *Neural ordinary differential equations*, in *Proceedings of the 32nd International Conference on Neural Information Processing Systems*, NIPS'18, (Red Hook, NY, USA), p. 6572–6583, Curran Associates Inc., 2018.
- [20] P. de Haan, C. Rainone, M.C.N. Cheng and R. Bondesan, *Scaling Up Machine Learning For Quantum Field Theory with Equivariant Continuous Flows*, 2110.02673.
- [21] M. Gerdes, P. de Haan, C. Rainone, R. Bondesan and M.C.N. Cheng, *Learning lattice quantum field theories with equivariant continuous flows*, *SciPost Phys.* **15** (2023) 238 [2207.00283].
- [22] M. Caselle, E. Cellini and A. Nada, *Sampling the lattice Nambu-Goto string using Continuous Normalizing Flows*, *Journal of High Energy Physics* **02** (2024) 048 [2307.01107].
- [23] H. Wu, J. Köhler and F. Noé, *Stochastic normalizing flows*, *Advances in Neural Information Processing Systems* **33** (2020) 5933.
- [24] M. Caselle, E. Cellini, A. Nada and M. Panero, *Stochastic normalizing flows as non-equilibrium transformations*, *JHEP* **07** (2022) 015 [2201.08862].

- [25] A. Bulgarelli, E. Cellini and A. Nada, *Scaling of Stochastic Normalizing Flows in SU(3) lattice gauge theory*, [2412.00200](#).
- [26] L. Del Debbio, J.M. Rossney and M. Wilson, *Efficient modeling of trivializing maps for lattice  $\phi_4$  theory using normalizing flows: A first look at scalability*, *Phys. Rev. D* **104** (2021) 094507 [[2105.12481](#)].
- [27] R. Abbott et al., *Aspects of scaling and scalability for flow-based sampling of lattice QCD*, *Eur. Phys. J. A* **59** (2023) 257 [[2211.07541](#)].
- [28] J. Komijani and M.K. Marinkovic, *Generative models for scalar field theories: how to deal with poor scaling?*, *PoS LATTICE2022* (2023) 019 [[2301.01504](#)].
- [29] R. Abbott et al., *Normalizing flows for lattice gauge theory in arbitrary space-time dimension*, [2305.02402](#).
- [30] K.A. Nicoli, C.J. Anders, T. Hartung, K. Jansen, P. Kessel and S. Nakajima, *Detecting and mitigating mode-collapse for flow-based sampling of lattice field theories*, *Phys. Rev. D* **108** (2023) 114501 [[2302.14082](#)].
- [31] V. Kanaujia, M.S. Scheurer and V. Arora, *AdvNF: Reducing mode collapse in conditional normalising flows using adversarial learning*, *SciPost Phys.* **16** (2024) 132 [[2401.15948](#)].
- [32] J. Sohl-Dickstein, E. Weiss, N. Maheswaranathan and S. Ganguli, *Deep unsupervised learning using nonequilibrium thermodynamics*, in *International conference on machine learning*, pp. 2256–2265, PMLR, 2015.
- [33] J. Ho, A. Jain and P. Abbeel, *Denoising diffusion probabilistic models*, *Advances in neural information processing systems* **33** (2020) 6840.
- [34] Y. Song and S. Ermon, *Generative modeling by estimating gradients of the data distribution*, *Advances in neural information processing systems* **32** (2019) [[1907.05600](#)].
- [35] Y. Song, J. Sohl-Dickstein, D.P. Kingma, A. Kumar, S. Ermon and B. Poole, *Score-based generative modeling through stochastic differential equations*, *arXiv preprint arXiv:2011.13456* (2020) .
- [36] L. Yang, Z. Zhang, Y. Song, S. Hong, R. Xu, Y. Zhao et al., *Diffusion models: A comprehensive survey of methods and applications*, *ACM Computing Surveys* **56** (2023) 1 [[2209.00796](#)].
- [37] F.-A. Croitoru, V. Hondru, R.T. Ionescu and M. Shah, *Diffusion models in vision: A survey*, *IEEE Transactions on Pattern Analysis and Machine Intelligence* **45** (2023) 10850 [[2209.04747](#)].
- [38] V. Mikuni and B. Nachman, *Score-based generative models for calorimeter shower simulation*, *Phys. Rev. D* **106** (2022) 092009 [[2206.11898](#)].
- [39] O. Amram and K. Pedro, *Denoising diffusion models with geometry adaptation for high fidelity calorimeter simulation*, *Phys. Rev. D* **108** (2023) 072014 [[2308.03876](#)].
- [40] V. Mikuni, B. Nachman and M. Pettee, *Fast point cloud generation with diffusion models in high energy physics*, *Phys. Rev. D* **108** (2023) 036025 [[2304.01266](#)].
- [41] P. Devlin, J.-W. Qiu, F. Ringer and N. Sato, *Diffusion model approach to simulating electron-proton scattering events*, *Phys. Rev. D* **110** (2024) 016030 [[2310.16308](#)].
- [42] C.M. Bishop and H. Bishop, *Deep learning: Foundations and concepts*, Springer Nature (2023).

- [43] L. Wang, G. Aarts and K. Zhou, *Diffusion models as stochastic quantization in lattice field theory*, *JHEP* **05** (2024) 060 [[2309.17082](#)].
- [44] L. Wang, G. Aarts and K. Zhou, *Generative Diffusion Models for Lattice Field Theory*, in *37th Conference on Neural Information Processing Systems*, 2023 [[2311.03578](#)].
- [45] G. Parisi, Y.S. Wu et al., *Perturbation theory without gauge fixing*, *Sci. sin* **24** (1981) 483.
- [46] P.H. Damgaard and H. Huffel, *Stochastic Quantization*, *Phys. Rept.* **152** (1987) 227.
- [47] M. Namiki, *Basic ideas of stochastic quantization*, *Prog. Theor. Phys. Suppl.* **111** (1993) 1.
- [48] K. Fukushima and S. Kamata, *Stochastic quantization and diffusion models*, *J. Phys. Soc. Jap.* **94** (2025) 031010 [[2411.11297](#)].
- [49] Y. Hirono, A. Tanaka and K. Fukushima, *Understanding diffusion models by feynman's path integral*, *arXiv preprint arXiv:2403.11262* (2024) .
- [50] G. Aarts, D.E. Habibi, L. Wang and K. Zhou, *On learning higher-order cumulants in diffusion models*, in *38th conference on Neural Information Processing Systems*, 2024 [[2410.21212](#)].
- [51] D.E. Habibi, G. Aarts, L. Wang and K. Zhou, *Diffusion models learn distributions generated by complex Langevin dynamics*, *PoS LATTICE2024* (2025) 039 [[2412.01919](#)].
- [52] Q. Zhu, G. Aarts, W. Wang, K. Zhou and L. Wang, *Diffusion models for lattice gauge field simulations*, in *38th conference on Neural Information Processing Systems*, 10, 2024 [[2410.19602](#)].
- [53] C. Gattringer and C.B. Lang, *Quantum chromodynamics on the lattice*, vol. 788, Springer, Berlin (2010), [10.1007/978-3-642-01850-3](#).
- [54] J. Greensite, *An introduction to the confinement problem*, vol. 821, Springer (2011), [10.1007/978-3-642-14382-3](#).
- [55] X. Crean, J. Giansiracusa and B. Lucini, *Topological data analysis of monopole current networks in  $U(1)$  lattice gauge theory*, *SciPost Phys.* **17** (2024) 100 [[2403.07739](#)].
- [56] S.R. Coleman, R. Jackiw and L. Susskind, *Charge Shielding and Quark Confinement in the Massive Schwinger Model*, *Annals Phys.* **93** (1975) 267.
- [57] S. Duane, A.D. Kennedy, B.J. Pendleton and D. Roweth, *Hybrid Monte Carlo*, *Phys. Lett. B* **195** (1987) 216.
- [58] R.M. Neal, *Handbook of Markov Chain Monte Carlo*, CRC Press (5, 2011), [10.1201/b10905](#), [[1206.1901](#)].
- [59] M.F. Atiyah and I.M. Singer, *The Index of elliptic operators. 1*, *Annals Math.* **87** (1968) 484.
- [60] S. Durr and P. Rouenhoff, *Topology in 2D non-Abelian Lattice Gauge Theories*, in *41st International Symposium on Lattice Field Theory*, 11, 2024 [[2411.11593](#)].
- [61] D. Albandea, P. Hernández, A. Ramos and F. Romero-López, *Improved topological sampling for lattice gauge theories*, *PoS LATTICE2021* (2022) 183 [[2111.05745](#)].
- [62] B. Alles, G. Boyd, M. D'Elia, A. Di Giacomo and E. Vicari, *Hybrid Monte Carlo and topological modes of full QCD*, *Phys. Lett. B* **389** (1996) 107 [[hep-lat/9607049](#)].
- [63] L. Del Debbio, H. Panagopoulos and E. Vicari, *theta dependence of  $SU(N)$  gauge theories*, *JHEP* **08** (2002) 044 [[hep-th/0204125](#)].

- [64] L. Del Debbio, G.M. Manca and E. Vicari, *Critical slowing down of topological modes*, *Phys. Lett. B* **594** (2004) 315 [[hep-lat/0403001](#)].
- [65] C. Bonanno, C. Bonati and M. D’Elia, *Topological properties of  $CP^{N-1}$  models in the large- $N$  limit*, *JHEP* **01** (2019) 003 [[1807.11357](#)].
- [66] ALPHA collaboration, *Critical slowing down and error analysis in lattice QCD simulations*, *Nucl. Phys. B* **845** (2011) 93 [[1009.5228](#)].
- [67] L. Del Debbio, H. Panagopoulos, P. Rossi and E. Vicari, *Spectrum of confining strings in  $SU(N)$  gauge theories*, *JHEP* **01** (2002) 009 [[hep-th/0111090](#)].
- [68] R.M. Neal, *Annealed importance sampling*, *Statistics and Computing* **11** (2001) .
- [69] G. Aarts, L. Wang and K. Zhou, *Diffusion models and stochastic quantisation in lattice field theory*, in *41st International Symposium on Lattice Field Theory*, 12, 2024 [[2412.13704](#)].
- [70] Y. Song, J. Sohl-Dickstein, D.P. Kingma, A. Kumar, S. Ermon and B. Poole, *Score-based generative modeling through stochastic differential equations*, *arXiv preprint arXiv:2011.13456* (2020) .
- [71] B.D. Anderson, *Reverse-time diffusion equation models*, *Stochastic Processes and their Applications* **12** (1982) 313.
- [72] A.M. Ferrenberg and R.H. Swendsen, *New Monte Carlo Technique for Studying Phase Transitions*, *Phys. Rev. Lett.* **61** (1988) 2635.
- [73] L. Wang, Y. Jiang and K. Zhou, *Neural network statistical mechanics*, [2007.01037](#).
- [74] T. Xu, L. Wang, L. He, K. Zhou and Y. Jiang, *Building imaginary-time thermal field theory with artificial neural networks*, *Chinese Physics C* **48** (2024) 1 [[2405.10493](#)].
- [75] G.O. Roberts and J.S. Rosenthal, *Optimal scaling of discrete approximations to Langevin diffusions*, *Journal of the Royal Statistical Society: Series B (Statistical Methodology)* **60** (1998) 255.
- [76] M. Girolami and B. Calderhead, *Riemann manifold langevin and hamiltonian monte carlo methods*, *Journal of the Royal Statistical Society Series B: Statistical Methodology* **73** (2011) 123.
- [77] M. Favoni, A. Ipp, D.I. Müller and D. Schuh, *Lattice Gauge Equivariant Convolutional Neural Networks*, *Phys. Rev. Lett.* **128** (2022) 032003 [[2012.12901](#)].
- [78] Y. Nagai and A. Tomiya, *Gauge covariant neural network for quarks and gluons*, [2103.11965](#).
- [79] Y. Nagai, H. Ohno and A. Tomiya, *CASK: A Gauge Covariant Transformer for Lattice Gauge Theory*, in *41st International Symposium on Lattice Field Theory*, 1, 2025 [[2501.16955](#)].
- [80] G. Aarts, K. Fukushima, T. Hatsuda, A. Ipp, S. Shi, L. Wang et al., *Physics-driven learning for inverse problems in quantum chromodynamics*, *Nature Reviews Physics* (2025) [[2501.05580](#)].
- [81] N. Madras and A.D. Sokal, *The Pivot algorithm: a highly efficient Monte Carlo method for selfavoiding walk*, *J. Statist. Phys.* **50** (1988) 109.
- [82] T.G. Kovacs, E.T. Tomboulis and Z. Schram, *Topology on the lattice: 2-d Yang-Mills theories with a theta term*, *Nucl. Phys. B* **454** (1995) 45 [[hep-th/9505005](#)].

- [83] C. Bonati and P. Rossi, *Topological susceptibility of two-dimensional  $U(N)$  gauge theories*, *Phys. Rev. D* **99** (2019) 054503 [[1901.09830](#)].
- [84] C. Bonati and P. Rossi, *Topological effects in continuum two-dimensional  $U(N)$  gauge theories*, *Phys. Rev. D* **100** (2019) 054502 [[1908.07476](#)].